PHYSICAL REVIEW D **80,** 095009 (2009)

Anomalous resonant production of the fourth-family up-type quarks at the LHC

İ. T. Çakır*
Department of Physics, CERN, 1211 Geneva 23, Switzerland

H. Duran Yıldız†
Department of Physics, Dumlupınar University, Faculty of Arts and Sciences, Kütahya, Turkey

O. Çakır‡
Department of Physics, CERN, 1211 Geneva 23, Switzerland
and Department of Physics, Faculty of Sciences, Ankara University, 06100, Tandogan, Ankara, Turkey

G. Ünel§
Department of Physics, CERN, 1211 Geneva 23, Switzerland
and Department of Physics, University of California at Irvine, Irvine, California, USA
(Received 12 August 2009; published 9 November 2009)

Considering the present limits on their masses from the Tevatron experiments, the fourth-family quarks are expected to have masses larger than the top quark. Because of their expected large masses, they could have different dynamics than the third-family quarks of the standard model. The resonant production of the fourth-family up-type quark t' has been studied via the anomalous production subprocess $gq_i \to t'$ (where $q_i = u, c$) at the LHC, with center-of-mass energies of 10 TeV and 14 TeV. The signatures of such a process are discussed within the standard model decay modes. The sensitivity to the anomalous coupling $\kappa/\Lambda = 0.1$ TeV^{-1} can be reached at $\sqrt{s} = 10$ TeV and $L_{\text{int}} = 100$ pb^{-1}.

DOI: 10.1103/PhysRevD.80.095009 PACS numbers: 12.60.−i, 13.85.Rm, 14.65.−q

I. INTRODUCTION

The number of fermion families in nature, the pattern of fermion masses, and the mixing angles in the quark/lepton sectors are unresolved issues in the standard model (SM). The repetition of quark and lepton families remains a mystery as part of the flavor problem. On theoretical grounds, the asymptotic freedom in quantum chromodynamics imposes an indirect bound on the number of quark flavors, which should be less than 18. The electroweak precision measurements done by the CERN LEP experiments imply that the number of light neutrinos ($m_\nu <$ 45 GeV) is equal to 3 [1]. The most recent analyses indicate that an additional family of heavy fermions is not inconsistent with the precision electroweak data at the available energies [2–8]. Indeed, the presence of three or four fermion families is equally consistent with the electroweak precision data; moreover the four-family scenario is favored if the Higgs boson is heavier than 200 GeV [4]. The fourth-family quarks have the Yukawa couplings running with the scale, and these couplings reach the Landau pole at just a little above 1 TeV. The discovery of the fourth-family quarks could reveal a dynamical symmetry breaking and mass formation via fermion condensation through strong interactions. The fourth family may play an important role in our understanding of the flavor structure of the SM. The flavor democracy is one of the main motivations for the existence of the fourth-family fermions [9]. Another motivation for the fourth family comes from the charge-spin unification [10]. Additional fermions can also be accommodated in many models beyond the SM [11]. A recent review of the fourth SM family, including the theoretical and experimental aspects, can be found in [12].

A lower limit on the mass of the fourth-family quark b' is $m_{b'} > 325$ GeV from Tevatron experiments [13], whereas the upper limit from partial wave unitarity is about 1 TeV. The recent results from the Collider Detector at Fermilab (CDF) exclude the t' mass below 311 GeV at 95% C.L. using the data of 2.8 fb^{-1} [14].

The tree-level flavor changing processes occur only via the charged current interactions in the SM. The first two rows of the Cabibbo-Kobayashi-Maskawa (CKM) matrix [15] are in good agreement with the unitary condition. The data for the number of b jets in top quark pair production at the Tevatron constrain the ratio $R = |V_{tb}|^2/\sum_q |V_{tq}|^2$, which is closely related to V_{tb} if the CKM is unitary. The direct constraints on $|V_{tb}|$ come from the single production of top quarks at the Tevatron. From the average cross section $\sigma = 3.94 \pm 0.88$ pb, the lower limit $|V_{tb}| > 0.78$ at 95% C.L. is given by the CDF and D0 Collaborations [16]. A measurement of the single top production cross section that is smaller than the SM prediction would imply $V_{tb} < 1$ or evidence of extra families of quarks mixed with the third generation. A flavor extension of the SM, with a

*tcakir@mail.cern.ch
†hyildiz@mail.cern.ch
‡ocakir@mail.cern.ch
§gokhan.unel@cern.ch

fourth generation of quarks, leads to an extended CKM matrix which could have V_{tb} smaller than 1. In the extended model, the strongest constraint on V_{tb} comes from the ratio $R_b = \Gamma(Z \to b\bar{b})/\Gamma(Z \to \text{hadrons})$, with $R > 0.9$ for $m_{t'} \geq 1.5 m_t$. For an extra up-type quark t' and another extra down-type quark b', the 4×4 matrix is unitary, for which any 3×3 submatrix becomes nonunitary as long as these new quarks mix with quarks of three families. Hence, the new flavor changing neutral currents (FCNC) could appear without violating the existing bounds from current experimental measurements [17,18].

The existence of a fourth generation of quarks would have interesting implications. Taking into account the current bounds on the mass of the fourth-family quarks [1], the anomalous interactions can emerge in the fourth family. Furthermore, extra families will yield an essential enhancement in the Higgs boson production at the LHC [19]. The single production [20,21] mechanism of fourth-family quarks will be suppressed by the elements (fourth row and/or fourth column) of the 4×4 CKM matrix. The fourth-family quark pairs can already be produced at the LHC at an initial center-of-mass energy of $\sqrt{s} = 10$ TeV and an initial luminosity of $L = 10^{31}\ \text{cm}^{-2}\,\text{s}^{-1}$. At the nominal center-of-mass energy $\sqrt{s} = 14$ TeV, the initial luminosity will be $10^{33}\ \text{cm}^{-2}\,\text{s}^{-1}$ which will later increase to $10^{34}\ \text{cm}^{-2}\,\text{s}^{-1}$ corresponding to 10 and 100 fb^{-1} per year, respectively.

In this work, we present an analysis of the anomalous resonant production of t' quarks at the LHC. Here, we assume the case t' decays through SM dominated channel (via charged currents) in which the magnitude of $V_{t'q}$ is important, leading to a final state $W^{\pm} b_{\text{jet}}$ for t' anomalous production. A fast simulation is performed for the detector effects on the signal and background. Any observations of the invariant mass peak in the interval 300–800 GeV with the final state containing $W^{\pm} b_{\text{jet}}$ can be interpreted as the signal for t' anomalous resonant production.

II. FOURTH-FAMILY QUARK INTERACTIONS

Fourth-family quarks can couple to charged weak currents by $W^{\pm}$ boson exchange, neutral weak currents by Z^0 boson exchange, electromagnetic currents by photon exchange, and strong color currents by gluon exchange. We include the fourth-family quarks in the enlarged framework (primed) of the SM. The interaction Lagrangian is given by

$$\begin{aligned} L' = & -g_e \sum_{Q'_i = b', t'} Q_{ei} \bar{Q}'_i \gamma^\mu Q'_i A_\mu - g_s \sum_{Q'_i = b', t'} \bar{Q}'_i T^a \gamma^\mu Q'_i G^a_\mu \\ & - \frac{g_e}{2 \cos\theta_w \sin\theta_w} \sum_{Q'_i = b', t'} \bar{Q}'_i \gamma^\mu (g^i_V - g^i_A \gamma^5) Q'_i Z^0_\mu \\ & - \frac{g_e}{2\sqrt{2} \sin\theta_w} \sum_{Q'_{i \neq j} = b', t'} V_{ij} \bar{Q}'_i \gamma^\mu (1 - \gamma^5) q_j W^{\pm}_\mu + \text{H.c.}, \end{aligned} \tag{1}$$

where g_e is the electromagnetic coupling constant and g_s is the strong coupling constant. The vector fields A_μ, G_μ, Z_μ, and $W^{\pm}_\mu$ denote the photon, gluon, Z^0 boson, and $W^{\pm}$ boson, respectively. Q_{ei} is the electric charge of fourth-family quarks, and T^a are the Gell-Mann matrices. The g_V and g_A are the couplings for vector and axial-vector neutral currents. Finally, the CKM matrix elements V_{ij} are expressed as $V = V^U V^{D\dagger}$. The corresponding 4×4 CKM matrix is given by

$$V = \begin{pmatrix} \mathbf{V_{ud}} & \mathbf{V_{us}} & \mathbf{V_{ub}} & V_{ub'} \\ \mathbf{V_{cd}} & \mathbf{V_{cs}} & \mathbf{V_{cb}} & V_{cb'} \\ \mathbf{V_{td}} & \mathbf{V_{ts}} & \mathbf{V_{tb}} & V_{tb'} \\ V_{t'd} & V_{t's} & V_{t'b} & V_{t'b'} \end{pmatrix}. \tag{2}$$

The magnitude of the 3×3 CKM matrix elements is determined from the low energy and high energy experiments: these are $|V_{ud}| = 0.974\,18 \pm 0.000\,27$, $|V_{us}| = 0.2255 \pm 0.0019$, $|V_{ub}| = 0.003\,93 \pm 0.000\,36$, $|V_{cd}| = 0.230 \pm 0.011$, $|V_{cs}| = 1.04 \pm 0.06$, $|V_{cb}| = 0.0412 \pm 0.0011$, $|V_{td}| = 0.0081 \pm 0.0006$, $|V_{ts}| = 0.0387 \pm 0.0023$ (assuming $|V_{tb}|$ is equal to unity) [1], and single top production yields $|V_{tb}| = 0.91 \pm 0.11$ at 95% C.L. [22]. In the fourth-family case, these elements should be less than their mean values. For a 4×4 CKM matrix, from the unitary requirement, the first three rows are calculated as $|V_{ub'}|^2 \leq 0.00011$, $|V_{cb'}|^2 \leq 0.13519$, and $|V_{tb'}|^2 \leq 0.295\,24$. For the first three columns one calculates the values $|V_{t'd}|^2 \leq 0.001\,99$, $|V_{t's}|^2 \leq 0.133\,95$, and $|V_{t'b}|^2 \leq 0.170\,19$. We see that there is a loose constraint for the mixing between third- and fourth-family quarks. Recent studies [23] have shown that CKM mixing between third-family quarks and fourth-family quarks can be as large as the Cabibbo mixing. The electroweak oblique parameters (S, T) are within the experimentally allowed regions if the fourth-family quarks have a mass splitting $|m_{t'} - m_{b'}| \gtrsim 50$ GeV [4]. In the case $m_{t'} \approx m_{b'} + 50$ GeV, the t' quark decay into $b' W^{+*}$ would be accessible, and this has some effects on the t' branchings depending on the CKM4 parametrization. When $m_{t'} \approx m_{b'} - 50$ GeV, we expect two-body decay for the t' quark. In this study, we consider mainly the latter option. Inspired by the Wolfenstein parametrization of the 3×3 CKM matrix, we could simply consider a parametrization for the fourth row and fourth column of the 4×4 CKM as $|V_{q_i b'}| \simeq |V_{t' q_j}| = A_{ij} \lambda^{4-n}$, where A_{ij} can be optimized for the quark flavors q_i and q_j; n is the family number and λ is a constant.

We consider the decay width of the t' quark through $t' \to W^+ q$, including the final state quark mass; we find

$$\Gamma(Q' \to W q) = \frac{1}{16} \frac{\alpha_e |V_{Q'q}|^2 m^3_{Q'}}{\sin^2\theta_W m^2_W} \lambda_W \sqrt{\lambda_r}, \tag{3}$$

where

$$\lambda_r = 1 + m_W^4/m_{Q'}^4 + m_q^4/m_{Q'}^4 - 2m_W^2/m_{Q'}^2 - 2m_q^2/m_{Q'}^2 - 2m_W^2 m_q^2/m_{Q'}^4 \quad (4)$$

$$\lambda_W = 1 + m_W^2/M_{Q'}^2 - 2m_q^2/m_{Q'}^2 + m_q^4/m_{Q'}^4 + m_q^2 m_W^2/m_{Q'}^4 - 2m_W^4/m_{Q'}^4. \quad (5)$$

To calculate the decay width numerically, we assume three parametrizations—PI, PII, and PIII—for the fourth-family mixing matrix elements. For the PI parametrization we assume the constant values $|V_{Q'q}| = |V_{qQ'}| = 0.01$, PII contains a dynamical parametrization $|V_{q_iQ'}| = |V_{Q'q_j}| \approx \lambda^{4-n}$ with a preferred value of $\lambda = 0.1$, and the PIII parametrization assumes maximal mixings $|V_{t'd}| \simeq 0.063$, $|V_{t's}| \simeq 0.46$, $|V_{t'b}| \simeq 0.47$, $|V_{ub'}| \simeq 0.044$, $|V_{cb'}| \simeq 0.46$, $|V_{tb'}| \simeq 0.47$, given by Ref. [24], corresponding to the case of one sigma deviation from the mean values of $|V_{Q'i}|^2$ and $|V_{iQ'}|^2$.

The flavor changing neutral current interactions are known to be absent at tree level in the SM. However, the fourth-family quarks, being heavier than the top quark, could have different dynamics than other quarks; they can couple to the FCNC currents, leading to an enhancement in the resonance processes at the LHC. Moreover, the arguments for the anomalous interactions of the top quark given in [25] are more valid for t' and b' quarks. The effective Lagrangian for the anomalous interactions among the fourth-family quarks t' and b', ordinary quarks q, and the neutral gauge bosons $V = \gamma, Z, g$ can be written explicitly:

$$L'_a = \sum_{q_i=u,c,t} \frac{\kappa_\gamma^{q_i}}{\Lambda} Q_{q_i} g_e \bar{t}' \sigma_{\mu\nu} q_i F^{\mu\nu} + \sum_{q_i=u,c,t} \frac{\kappa_z^{q_i}}{2\Lambda} g_z \bar{t}' \sigma_{\mu\nu} q_i Z^{\mu\nu} + \sum_{q_i=u,c,t} \frac{\kappa_g^{q_i}}{2\Lambda} g_s \bar{t}' \sigma_{\mu\nu} \lambda_a q_i G_a^{\mu\nu} + \text{H.c.}$$
$$+ \sum_{q_i=d,s,b} \frac{\kappa_\gamma^{q_i}}{\Lambda} Q_{q_i} g_e \bar{b}' \sigma_{\mu\nu} q_i F^{\mu\nu} + \sum_{q_i=d,s,b} \frac{\kappa_z^{q_i}}{2\Lambda} g_z \bar{b}' \sigma_{\mu\nu} q_i Z^{\mu\nu} + \sum_{q_i=d,s,b} \frac{\kappa_g^{q_i}}{2\Lambda} g_s \bar{b}' \sigma_{\mu\nu} \lambda_a q_i G_a^{\mu\nu} + \text{H.c.}, \quad (6)$$

where $F^{\mu\nu}$, $Z^{\mu\nu}$, and $G^{\mu\nu}$ are the field strength tensors of the gauge bosons; $\sigma_{\mu\nu} = i(\gamma_\mu\gamma_\nu - \gamma_\nu\gamma_\mu)/2$; λ_a are the Gell-Mann matrices; Q_q is the electric charge of the quark (q); g_e, g_Z, and g_s are the electromagnetic, neutral weak, and strong coupling constants, respectively. $g_Z = g_e/\cos\theta_w \sin\theta_w$, where θ_w is the weak angle. κ_γ is the anomalous coupling with the photon, κ_z is for the Z boson, and κ_g is the coupling with the gluon. Λ is the scale for new interactions.

For the decays $Q' \to Vq$, where $V \equiv \gamma, Z, g$, we use the effective Lagrangian to calculate the anomalous decay widths,

$$\Gamma(Q' \to gq) = \frac{2}{3}\left(\frac{\kappa_g^q}{\Lambda}\right)^2 \alpha_s m_{Q'}^3 \lambda_0, \quad (7)$$

$$\Gamma(Q' \to \gamma q) = \frac{1}{2}\left(\frac{\kappa_\gamma^q}{\Lambda}\right)^2 \alpha_e Q_q^2 m_{Q'}^3 \lambda_0, \quad (8)$$

$$\Gamma(Q' \to Zq) = \frac{1}{16}\left(\frac{\kappa_Z^q}{\Lambda}\right)^2 \frac{\alpha_e m_{Q'}^3}{\sin^2\theta_W \cos^2\theta_W} \lambda_Z \sqrt{\lambda_r}, \quad (9)$$

with

$$\lambda_0 = 1 - 3m_q^2/m_{Q'}^2 + 3m_q^4/m_{Q'}^4 - m_q^6/m_{Q'}^6, \quad (10)$$

$$\lambda_Z = 2 - m_Z^2/m_{Q'}^2 - 4m_q^2/m_{Q'}^2 + 2m_q^4/m_{Q'}^4 - 6m_q m_Z^2/m_{Q'}^3 - m_Z^2 m_t^2/m_{Q'}^4 - m_Z^4/m_{Q'}^4. \quad (11)$$

The anomalous decay widths in different channels are proportional to Λ^{-2}, and they begin to contribute more when $\kappa/\Lambda > 0.1$ TeV^{-1}.

The total decay width of the t' quark is shown in Fig. 1. In Table I, we give the numerical values of the total decay width and branching ratios for the parametrizations PI–PIII. As it can be seen from these tables, for the mass range of $m_{t'}$ relevant to LHC experiments, the fractions of

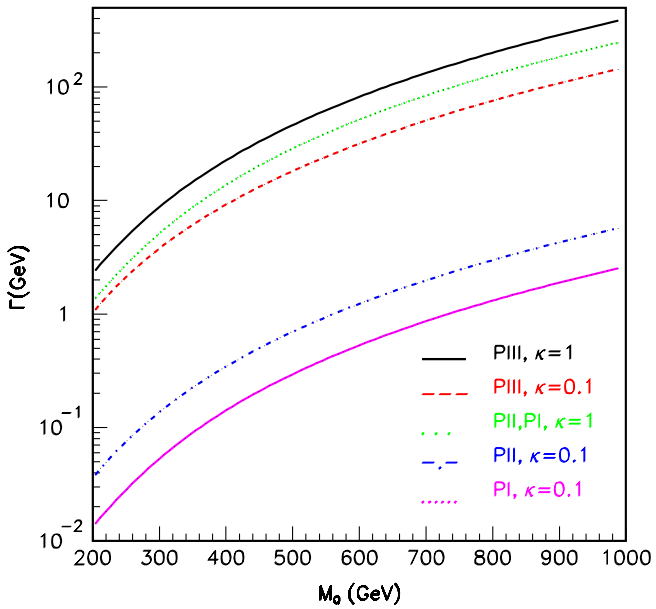

FIG. 1 (color online). Decay width of the t' quark depending on its mass for different $V_{t'q}$ parametrizations and κ/Λ values.

TABLE I. Decay widths and branching ratios (%) of the fourth-family quarks in both chiral and anomalous interactions, where q_i denotes the quarks belonging to the ith family. $Vq_{1,2}$ denotes Vq_1 and Vq_2. The parametrizations for the 4×4 CKM elements are taken as PI, PII, PIII, as given in the text. In the last row the total decay widths of fourth-family t' quarks are given for three mass values and $\kappa/\Lambda = 1$ TeV^{-1}. The numbers in the parentheses denote the values for $\kappa/\Lambda = 0.1$ TeV^{-1}.

	PI			PII			PIII		
$m_{t'}$ (GeV)	300	500	700	300	500	700	300	500	700
Wq_1	0.017(1.6)	0.014(1.4)	0.014(1.3)	0.0002(0.0062)	0.0001(0.0059)	0.0001(0.0058)	0.39(0.9)	0.35(0.9)	0.34(0.89)
Wq_2	0.017(1.6)	0.014(1.4)	0.014(1.3)	0.017(0.62)	0.014(0.59)	0.014(0.58)	21.0(48)	19.0(48)	18.0(48)
Wq_3	0.017(1.6)	0.014(1.4)	0.014(1.3)	1.7(62)	1.4(59)	1.4(58)	21.0(50)	20.0(50)	19.0(50)
$Zq_{1,2}$	2.5(2.3)	2.3(2.2)	2.2(2.1)	2.4(0.91)	2.3(0.93)	2.2(0.93)	1.4(0.033)	1.4(0.036)	1.4(0.037)
Zq_3	0.27(0.26)	1.4(1.4)	1.8(1.7)	0.27(0.1)	1.4(0.59)	1.8(0.75)	0.16(0.0036)	0.89(0.023)	1.1(0.03)
$\gamma q_{1,2}$	0.9(0.86)	0.76(0.73)	0.72(0.69)	0.89(0.33)	0.75(0.31)	0.71(0.3)	0.52(0.012)	0.47(0.012)	0.45(0.012)
γq_3	0.26(0.25)	0.52(0.5)	0.6(0.57)	0.26(0.097)	0.51(0.21)	0.59(0.25)	0.52(0.0035)	0.32(0.008)	0.37(0.0098)
$gq_{1,2}$	40(39)	34(33)	32(31)	40(15)	34(14)	32(14)	23.0(0.54)	21.0(0.53)	20.0(0.53)
gq_3	12(11)	23(22)	27(26)	12(4.4)	23(9.4)	26(11)	6.8(0.16)	14.0(0.36)	20.0(0.44)
Γ_{tot} (GeV)	5.21(0.055)	28.47(0.297)	82.58(0.859)	5.298(0.141)	28.871(0.701)	83.71(1.97)	9.05(3.89)	46.46(18.29)	132.04(50.30)

the anomalous decay modes are 99.9% (95%–96%), 98%(37%–41%), and 58%–62%(99%) at $\kappa/\Lambda = 1(0.1)$ TeV^{-1} for the parametrizations PI, PII, and PIII, respectively. However, SM decay modes of t' become dominant at PII and PIII parametrizations when $\kappa/\Lambda = 0.1$ TeV^{-1}. For the parametrization PIII, the SM decay mode and anomalous decay mode become comparable for $\kappa/\Lambda = 1$ TeV^{-1}.

If the CKM unitarity is strictly applied and the Q' mixing with light quarks is strongly constrained, which corresponds to $|V_{t'q_i}| \simeq 0$ for the light quarks q_i, there still remains room for the SM decays $t' \to W^+ b$ and the possible anomalous decays $t' \to Vq_i$. In this case, t' can have significant FCNC couplings. When the anomalous interactions greatly dominate over the SM decays, still allowing only the nonvanishing element $|V_{t'b'}| \simeq 1$ (but assuming t' and b' are mass degenerate), the decay widths and branching ratios of the fourth-family quarks with the anomalous interactions are shown in Table II. Taking the anomalous coupling $\kappa/\Lambda = 0.1$ TeV^{-1}, we calculate the t' anomalous decay widths $\Gamma = 8.79 \times 10^{-2}$ GeV, $\Gamma = 3.86 \times 10^{-1}$ GeV, and $\Gamma = 1.02$ GeV for $m_{t'} = 350$, 550, and 750 GeV, respectively.

TABLE II. Decay widths and branching ratios (%) of the fourth-family quarks with only anomalous interactions, where q_i denotes the quarks belonging to the ith family. $Vq_{1,2}$ denotes Vq_1 and Vq_2. In the last row the total decay widths of fourth-family t' and b' quarks are given for three mass values and $\kappa/\Lambda = 1$ TeV^{-1}.

	t'		
Mass (GeV)	300	500	700
$Zq_{1,2}$	2.5	2.3	2.2
Zq_3	0.27	1.4	1.8
$\gamma q_{1,2}$	0.9	0.76	0.72
γq_3	0.26	0.52	0.6
$gq_{1,2}$	40.0	34.0	32.0
gq_3	12.0	23.0	27.0
Γ_{tot} (GeV)	5.21	28.4	82.56

III. ANOMALOUS RESONANT PRODUCTION OF t' QUARKS

In order to study the resonant production of fourth-family quarks, we have implemented the anomalous interaction vertices with the new particles t' into the COMPHEP package [26]. In all numerical calculations, the parton distribution functions (PDF) $f_q(x, Q^2)$ and $f_g(y, Q^2)$ are set to the CTEQ6M parametrization [27] and the factorization scale $Q^2 = m_{Q'}^2$ is used. The total cross section for the process $pp \to W^+ bX$ is given by

$$\sigma = \int_{\tau_{\min}}^1 d\tau \int_\tau^1 \frac{dx}{x} f_q(x, Q^2) f_g\left(\frac{\tau}{x}, Q^2\right) \hat{\sigma}(\tau s), \qquad (12)$$

where $\hat{s} = \tau s$ and $\tau_{\min} = (m_V + m_q)^2/s$; $\hat{\sigma}$ is the partonic cross section for a given process. We consider the production $qg \to t'$ and the decay $t \to W^+ b_j$. In the generic

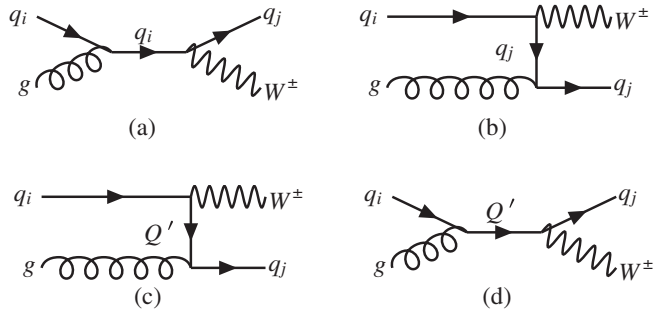

FIG. 2. Diagrams for the $gq_i \to W^+ q_j$ subprocess including $Q'qg$ (where $Q' \equiv t'$) anomalous vertices; q_i can be any of the quarks inside the proton, while q_j can be any of the quark flavors depending on the charged current interaction. For the $W^- \bar{q}_j$ final states we may change the direction of the current lines and replace the incoming antiquarks.

TABLE III. Resonance cross sections (pb) and decay widths of t' quarks for PI parametrization with $\kappa/\Lambda = 1$ TeV^{-1} and $\kappa/\Lambda = 0.1$ TeV^{-1} at $\sqrt{s} = 14(10)$ TeV.

	$\kappa/\Lambda = 1$ TeV^{-1}			$\kappa/\Lambda = 0.1$ TeV^{-1}		
$m_{t'}$ (GeV)	$\sigma(t')$	$\sigma(\bar{t}')$	$\Gamma_{t'}$ (GeV)	$\sigma(t')$	$\sigma(\bar{t}')$	$\Gamma_{t'}$ (GeV)
300	2.55(0.16)	$0.744(1.73 \times 10^{-3})$	5.21	2.53(0.149)	$0.693(1.65 \times 10^{-2})$	0.055
400	$1.43(6.11 \times 10^{-2})$	$0.360(5.16 \times 10^{-3})$	13.74	1.34(0.063)	$0.341(5.02 \times 10^{-3})$	0.143
500	$0.903(2.68 \times 10^{-2})$	$0.198(1.81 \times 10^{-3})$	28.46	0.856(0.027)	$0.192(1.77 \times 10^{-3})$	0.296
600	$0.608(1.26 \times 10^{-2})$	$0.119(7.07 \times 10^{-4})$	50.91	0.582(0.013)	$0.114(6.84 \times 10^{-4})$	0.530
700	$0.429(6.25 \times 10^{-3})$	$0.075(3.0 \times 10^{-4})$	82.59	0.415(0.006)	$0.075(2.84 \times 10^{-4})$	0.859
800	$0.311(3.2 \times 10^{-3})$	$0.049(1.38 \times 10^{-4})$	125.06	0.305(0.003)	$0.051(1.22 \times 10^{-4})$	1.30
900	$0.232(1.69 \times 10^{-3})$	$0.034(6.82 \times 10^{-5})$	179.82	$0.217(1.7 \times 10^{-3})$	$0.035(5.38 \times 10^{-5})$	1.86
1000	$0.174(9.24 \times 10^{-4})$	$0.023(3.66 \times 10^{-5})$	248.43	$0.178(8.8 \times 10^{-4})$	$0.025(2.39 \times 10^{-5})$	2.58

TABLE IV. Resonance cross sections (pb) and decay widths of t' quarks for PII parametrization with $\kappa/\Lambda = 1$ TeV^{-1} and $\kappa/\Lambda = 0.1$ TeV^{-1} at $\sqrt{s} = 14(10)$ TeV.

	$\kappa/\Lambda = 1$ TeV^{-1}			$\kappa/\Lambda = 0.1$ TeV^{-1}		
$m_{t'}$ (GeV)	$\sigma(t')$	$\sigma(\bar{t}')$	$\Gamma_{t'}$ (GeV)	$\sigma(t')$	$\sigma(\bar{t}')$	$\Gamma_{t'}$ (GeV)
300	250.92(15.48)	73.30(1.71)	5.29	93.24(5.87)	27.51(0.65)	0.14
400	141.24(6.02)	35.53(0.52)	13.94	55.62(2.44)	14.18(0.21)	0.35
500	88.89(2.64)	19.61(0.18)	28.87	36.26(1.12)	$8.18(7.48 \times 10^{-2})$	0.70
600	60.00(1.25)	$11.79(6.98 \times 10^{-2})$	51.61	25.16(0.55)	$5.06(2.95 \times 10^{-2})$	1.23
700	42.33(0.62)	$7.46(2.96 \times 10^{-2})$	83.71	18.14(0.28)	$3.29(1.23 \times 10^{-2})$	1.97
800	30.77(0.32)	$4.92(1.36 \times 10^{-2})$	126.72	13.45(0.14)	$2.23(5.35 \times 10^{-3})$	2.96
900	22.84(0.17)	$3.34(6.76 \times 10^{-3})$	182.18	10.22(0.075)	$1.55(2.37 \times 10^{-3})$	4.23
1000	$17.23(9.1 \times 10^{-2})$	$2.32(3.6 \times 10^{-3})$	251.67	7.92(0.039)	$1.11(1.07 \times 10^{-3})$	5.82

notation the contributing Feynman diagrams are shown in Fig. 2.

The production cross sections as a function of the fourth-family quark mass for the different parametrizations are shown in Tables III, IV, and V. The ratios of the cross sections for different parametrizations are calculated as $k_\sigma \approx 0.01$ for PI and $k_\sigma \approx 15$ for PIII with the normalization to PII with $\kappa/\Lambda = 1$ TeV^{-1}, as shown in Fig. 3. For the parametrization PIII we find the t' ($\bar{t}'$) production cross sections 46.4 (11.7) pb for $\kappa/\Lambda = 0.1$ TeV^{-1} and $m_{t'} = 400$ GeV at $\sqrt{s} = 14$ TeV. The $\bar{t}'$ production cross section is lower than t' production by a factor of 2–8 depending on the considered mass range. The general behavior of the cross sections depending on the mass is presented in Figs. 4–6.

IV. SIGNAL AND BACKGROUND

The resonant production mechanisms of the fourth-family t' quarks depend on the anomalous coupling κ/Λ, while their anomalous decays and charged current decays depend on both these couplings and the 4×4 CKM matrix elements. The signal process $pp \to W^+ bX$ includes t' exchange in the s channel. The s-channel contribution to

TABLE V. Resonance cross sections (pb) and decay widths of t' quarks for PIII parametrization with $\kappa/\Lambda = 1$ TeV^{-1} and $\kappa/\Lambda = 0.1$ TeV^{-1} at $\sqrt{s} = 14(10)$ TeV.

	$\kappa/\Lambda = 1$ TeV^{-1}			$\kappa/\Lambda = 0.1$ TeV^{-1}		
$m_{t'}$ (GeV)	$\sigma(t')$	$\sigma(\bar{t}')$	$\Gamma_{t'}$ (GeV)	$\sigma(t')$	$\sigma(\bar{t}')$	$\Gamma_{t'}$ (GeV)
300	3272.60(198.72)	946.54(21.92)	9.05	75.28(4.66)	22.03(0.515)	3.89
400	1912.50(79.96)	475.42(6.75)	22.92	46.43(2.00)	11.74(0.169)	9.33
500	1228.70(35.57)	267.17(2.42)	46.46	30.89(0.93)	$6.87(6.26 \times 10^{-2})$	18.28
600	835.63(16.85)	161.31(0.96)	82.03	21.60(0.46)	$4.28(2.53 \times 10^{-2})$	31.65
700	590.53(8.34)	102.24(0.42)	132.04	15.61(0.23)	$2.78(1.1 \times 10^{-2})$	50.30
800	428.19(4.27)	67.04(0.20)	198.88	11.56(0.12)	$1.87(4.95 \times 10^{-3})$	75.12
900	315.96(2.26)	$45.14(9.96 \times 10^{-2})$	284.95	8.73(0.064)	$1.29(2.39 \times 10^{-3})$	106.99
1000	236.33(1.25)	$30.94(5.53 \times 10^{-2})$	392.65	6.69(0.035)	$0.92(1.23 \times 10^{-3})$	146.79

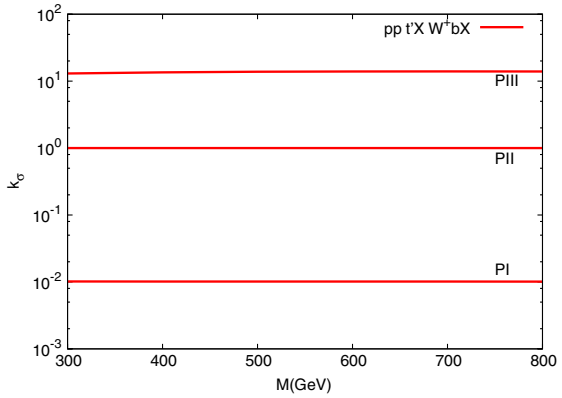

FIG. 3 (color online). The ratio of the cross sections for different parametrizations normalized to PII, where $\kappa/\Lambda = 1$ TeV^{-1}.

the signal process would manifest itself as resonance around the t' mass value in the W-boson + jet reconstructed invariant mass. When we consider the leptonic W decays, the t' signal search will be $\ell^+ + b_{\text{jet}} + \not{E}_T$, where $\ell = e,\ \mu$. For the hadronic W decays one would seek the events with one b jet alongside two more jets, requiring these to have an invariant mass peak around the W mass. If we consider the dominance of the SM decay mode over the anomalous decay, the t' resonant production signal will be

$$pp \to t'(\bar{t}')X, \qquad t'(\bar{t}') \to W^{+(-)} b_{\text{jet}} \quad \text{or} \quad W^{+(-)} j, \tag{13}$$

which includes further leptonic or hadronic decays of the

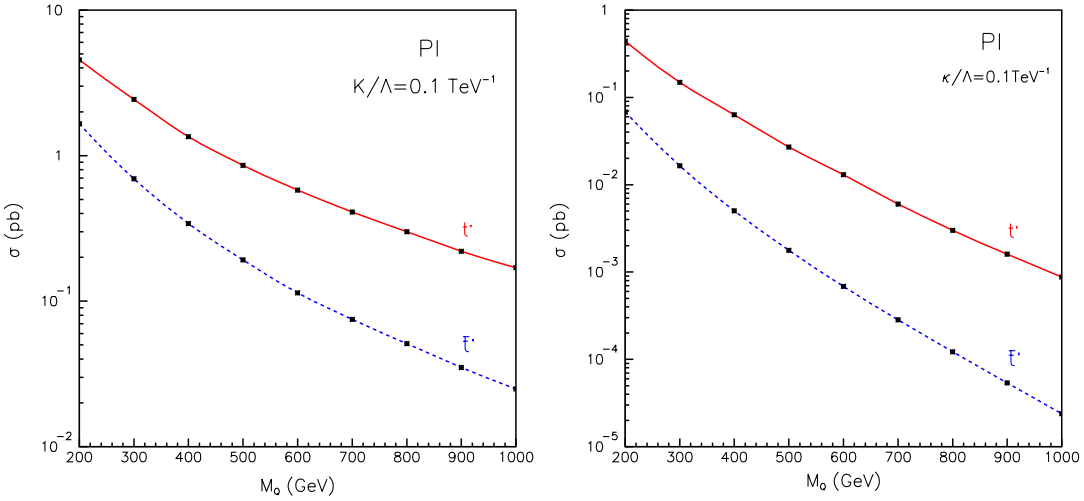

FIG. 4 (color online). The cross section for the anomalous production of t' quarks for the PI parametrization and $\kappa/\Lambda = 0.1$ TeV^{-1}. The lines denote $t'(\bar{t}')$ followed by the decay $W^+ b(W^- \bar{b})$ at the center-of-mass energy 14 TeV (left panel) and 10 TeV (right panel).

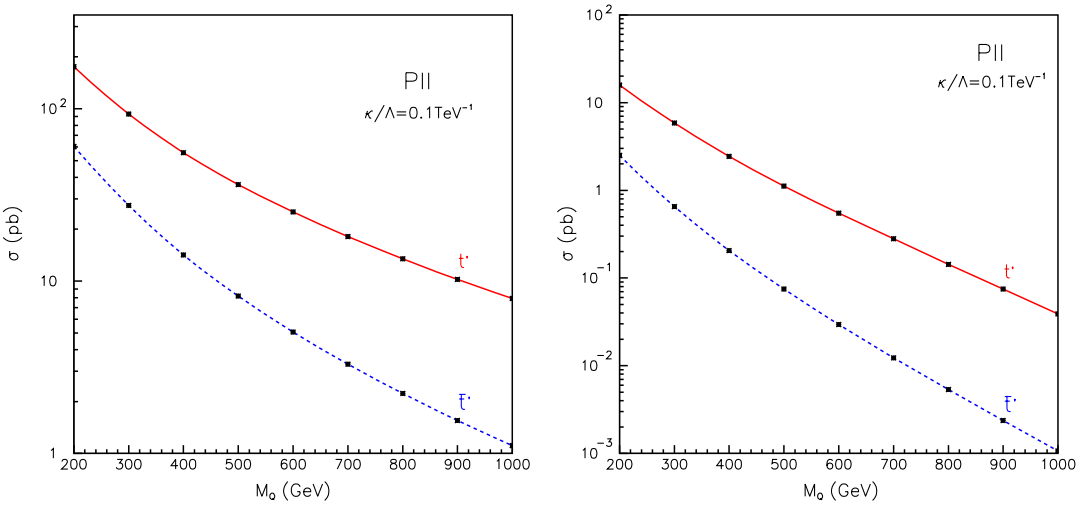

FIG. 5 (color online). The cross section for the anomalous production of t' quarks for the PII parametrization and $\kappa/\Lambda = 0.1$ TeV^{-1}. The lines denote $t'(\bar{t}')$ production followed by the decay $W^+ b(W^- \bar{b})$ at the center-of-mass energy 14 TeV (left panel) and 10 TeV (right panel).

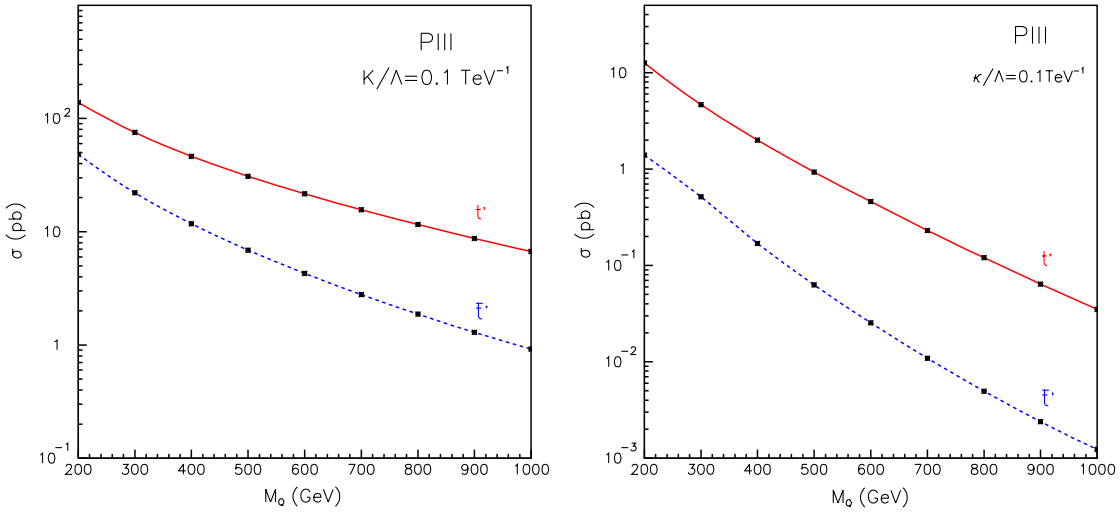

FIG. 6 (color online). The cross section for the anomalous production of t' quarks for the PIII parametrization and $\kappa/\Lambda = 0.1\ \mathrm{TeV}^{-1}$. The lines denote $t'(\bar{t}')$ production followed by the decay $W^+b(W^-\bar{b})$ at the center-of-mass energy 14 TeV (left panel) and 10 TeV (right panel).

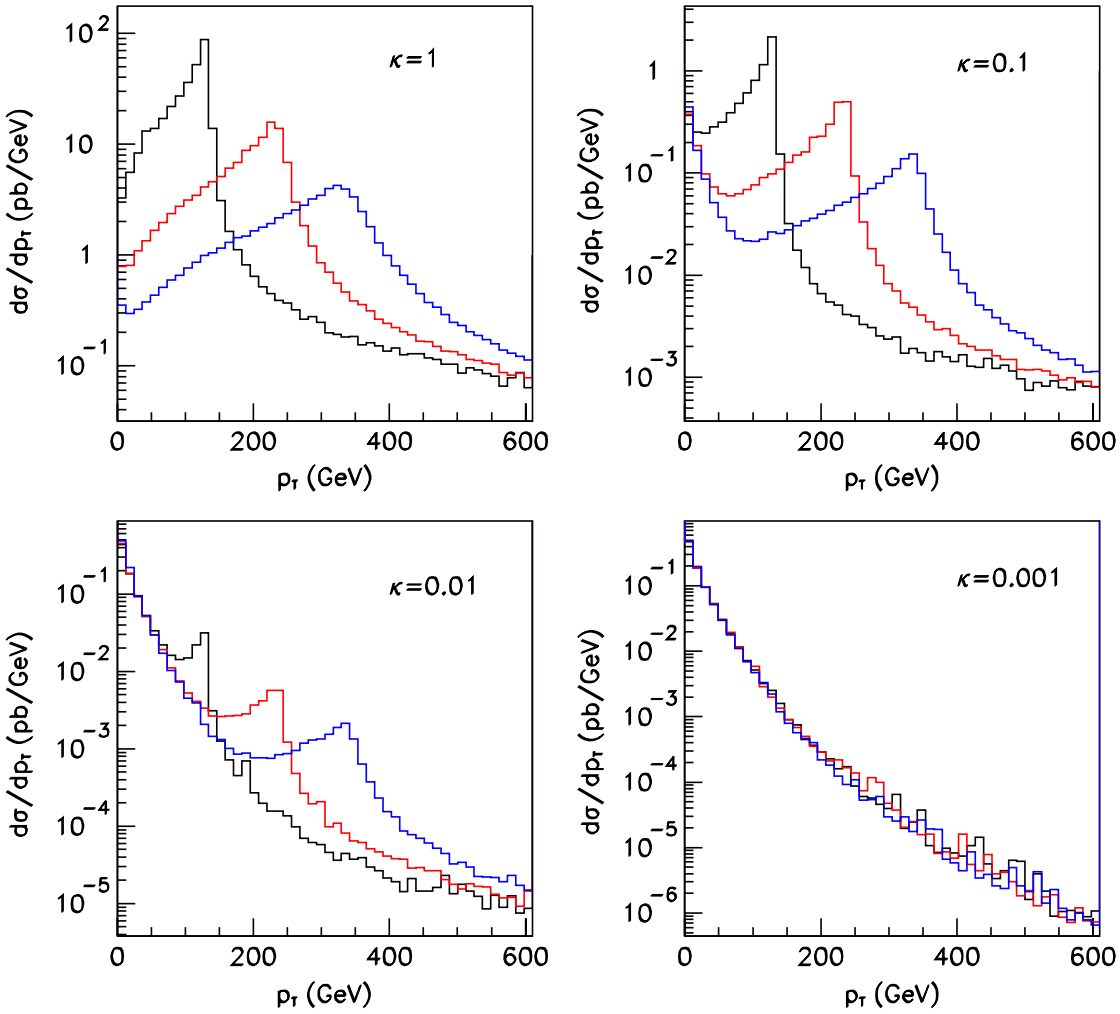

FIG. 7 (color online). Partonic-level p_T distributions of b quarks from the signal + background process $pp \to W^+bX$ at $\sqrt{s} = 14$ TeV. Here, the scale is taken as $\Lambda = 1$ TeV. The peaks occur around respective half mass values of the t' quark masses.

TABLE VI. Cross sections for the backgrounds ($W^{\pm}b$ and $W^{\pm}j$) with p_T cuts at the center-of-mass energy $\sqrt{s} = 14$ TeV.

Backgrounds	$p_T > 20$ GeV	$p_T > 50$ GeV	$p_T > 100$ GeV
$W^+b(W^-\bar{b})$	2.79(2.71)	$6.98 \times 10^{-1}(6.71 \times 10^{-1})$	$1.16 \times 10^{-1}(1.09 \times 10^{-1})$
$W^+j(W^-j)$	$2.22 \times 10^4(1.64 \times 10^4)$	$5.37 \times 10^3(3.87 \times 10^3)$	$1.02 \times 10^3(6.92 \times 10^2)$

W^+ boson. In the second and third lines, the elements of the 4×4 CKM matrix, $V_{t'b}$ and $V_{t'q}$, enter the decay process for the t' signal. The cross section for the SM process $pp \to W^+bX$ ($pp \to W^-\bar{b}X$) is 10.14 pb (9.78 pb) without any cuts at 14 TeV, and 5.73 pb (5.49 pb) at 10 TeV. For the cross section estimates, we assume the efficiency for b tagging to be $\varepsilon_b = 50\%$, and rejection factors $r_j = 100$ for light jets, and $r_c = 10$ for $c(\bar{c})$ quark jets since they are assumed to be mistagged as b jets. The p_T distributions for both signal and background are given in Fig. 7, including the interference terms. Moreover, different background processes contributing to the same final state are presented in Table VI with various p_T cuts. At the center-of-mass energy $\sqrt{s} = 10$ TeV, the background cross sections are calculated as 0.375 pb (0.354 pb) for W^+b (W^-b), and 2.69×10^3 pb (1.88×10^3 pb) for W^+j (W^-j) with $p_T^j > 50$ GeV. The invariant mass distributions of the $b\ell\nu$ system at partonic level for

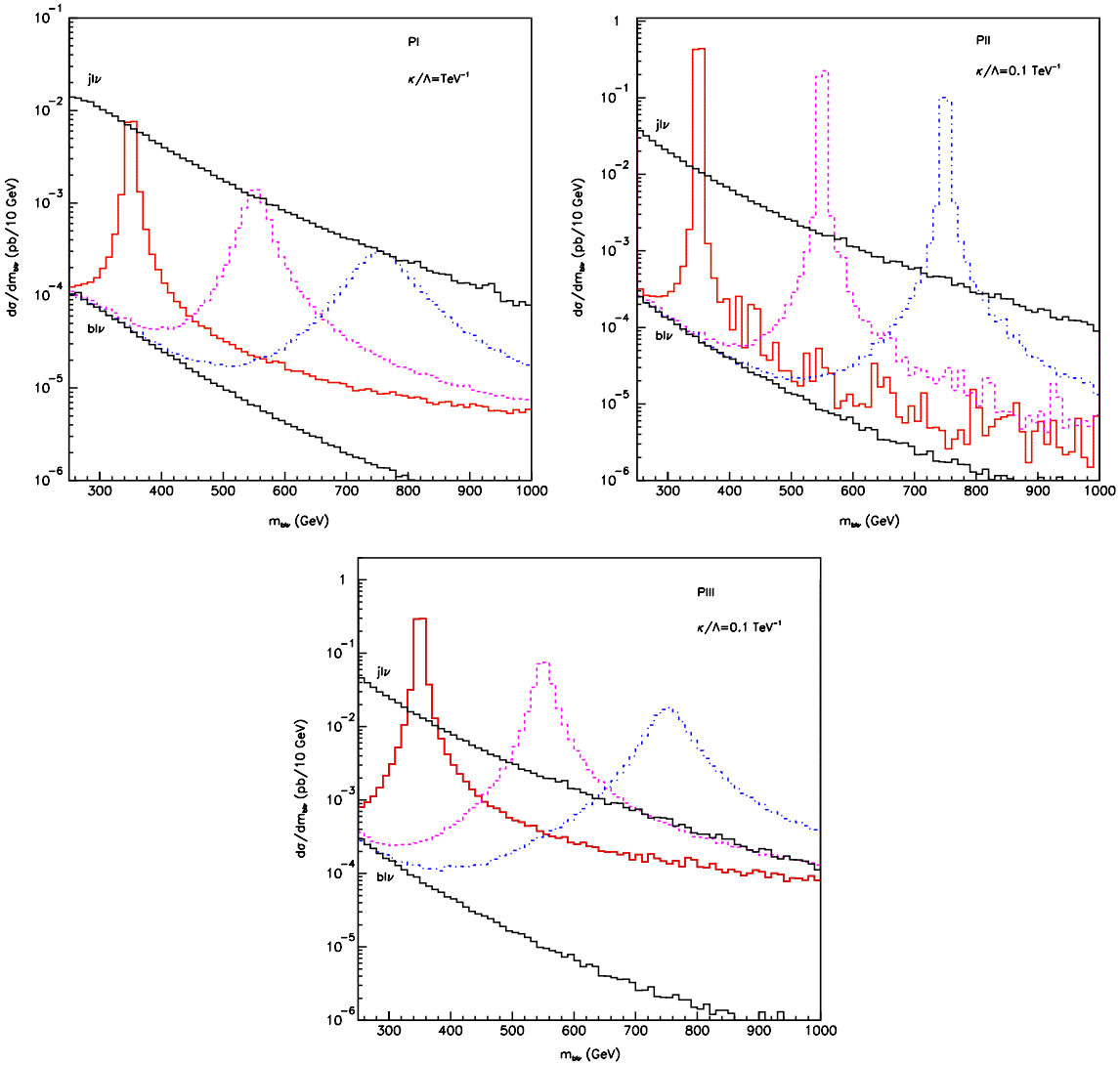

FIG. 8 (color online). Invariant mass distributions of the $b\ell\nu$ system at partonic level for PI (with $p_T^{b,j} > 100$ GeV), PII (with $p_T^{b,j} > 50$ GeV), and PIII (with $p_T^{b,j} > 50$ GeV) parametrizations at $\sqrt{s} = 14$ TeV.

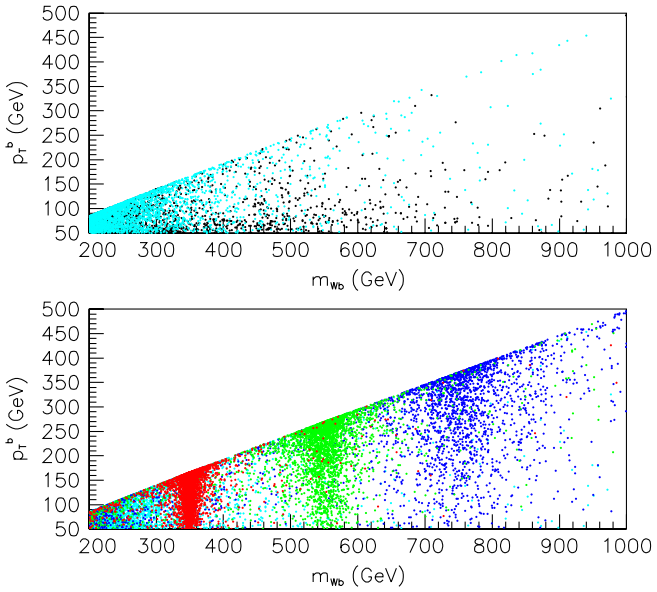

FIG. 9 (color online). Transverse momentum of the b jet versus W^+b invariant mass at $\sqrt{s} = 14$ TeV. On the upper panel only the background distribution with W^+b (black) and $W^+j(b)$ (cyan) events is shown, while on the lower panel both the background and signal distributions with masses of 350 (red), 550 (green), and 750 GeV (blue) are shown. Here, the anomalous coupling is taken to be $\kappa/\Lambda = 1$ TeV^{-1} and the mixing with the fourth-family quark t' is parametrized as the PII.

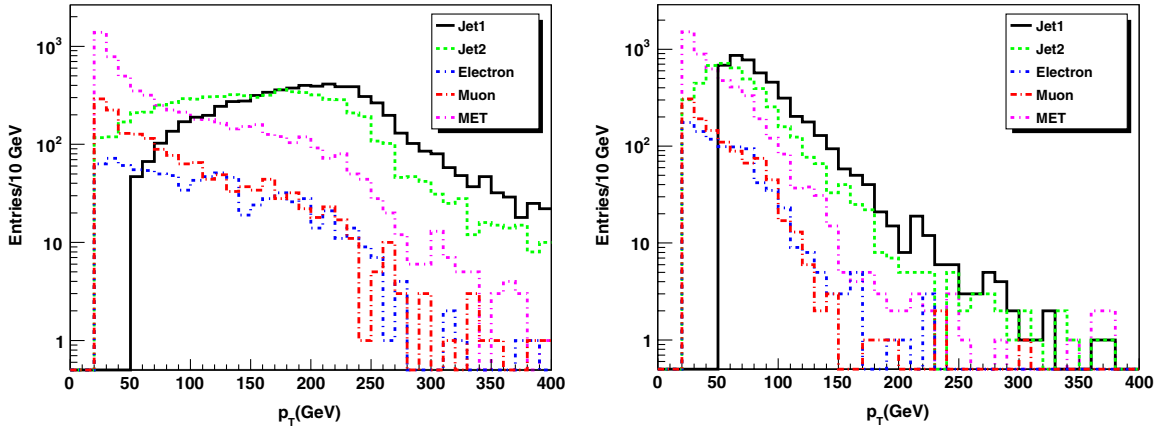

FIG. 10 (color online). The p_T distributions of jets, electrons, and muons from the signal ($t' \to W^+b$, left panel) and background (W^+b, right panel) after detector simulation. The jets are ordered according to the magnitude of their transverse momenta; here we apply the cuts $p_T^{j_1} > 50$ GeV, $p_T^{j_{2,3}} > 20$ GeV, $p_T^{\ell} > 20$ GeV, and $\not{E}_T > 20$ GeV.

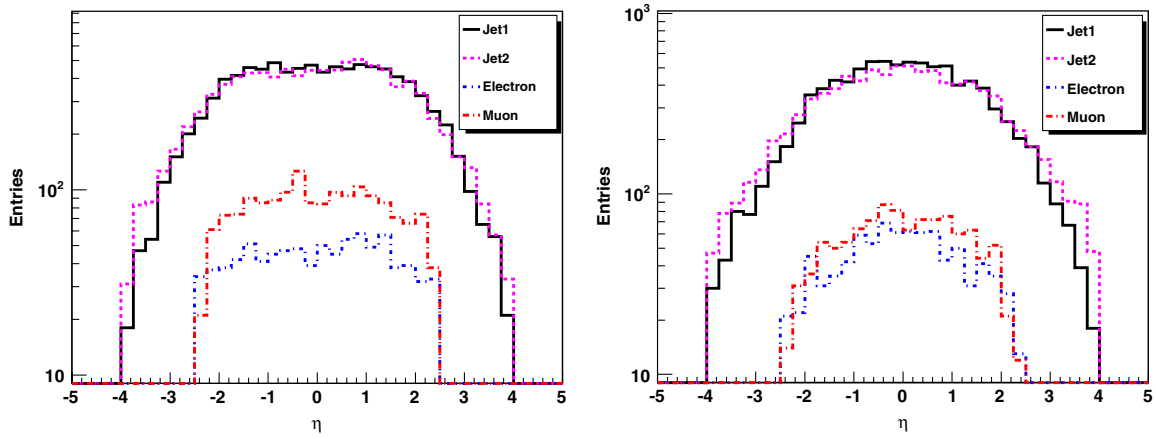

FIG. 11 (color online). The η distributions of jets, electrons, and muons from the simulated signal ($t' \to W^+b$, left panel) and background (W^+b, right panel). The jets are ordered according to the magnitude of their p_T. Typical LHC detectors have the acceptance for $|\eta| < 2.5$ when utilization of the inner tracker is imposed.

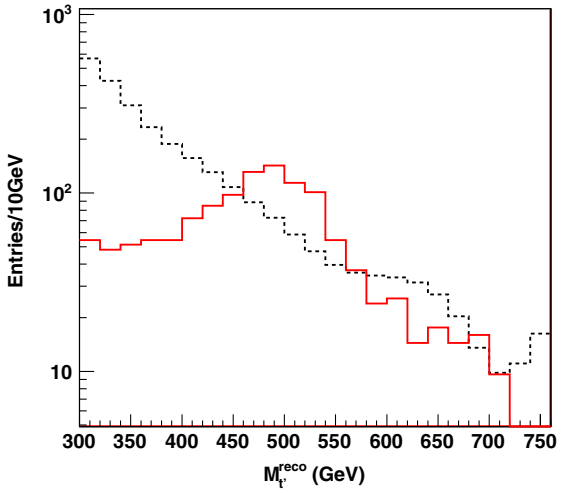

FIG. 12 (color online). Invariant mass distribution of the $b\ell\nu$ system for both signal ($\kappa/\Lambda = 0.1$ TeV^{-1}) and background at $\sqrt{s} = 14$ TeV.

different parametrizations are given in Fig. 8. Here, the W^+b and W^+j backgrounds are included with the assumed efficiencies and acceptance factors. In Fig. 9, we show a density plot of the transverse momentum of the b quark and the invariant mass distribution of the W^+b system with the t' mass constraint.

V. ANALYSIS

At the generator level, we have required a b jet with transverse momentum of at least $p_T^b > 50$ GeV for the W^+b events. The events generated for each subprocess are mixed using the *"mix"* script which can be found in the COMPHEP package [26], and passed to the PYTHIA [28] for further decays and hadronization using the CPYTH package [29]. After W-boson decay and hadronization, the detector effects, such as acceptance and resolution, are simulated with the PGS4 program [30] using generic LHC detector [31] parameters. This fast simulation includes the most important detector effects, such as p_T smearing, $E_{\rm em}$

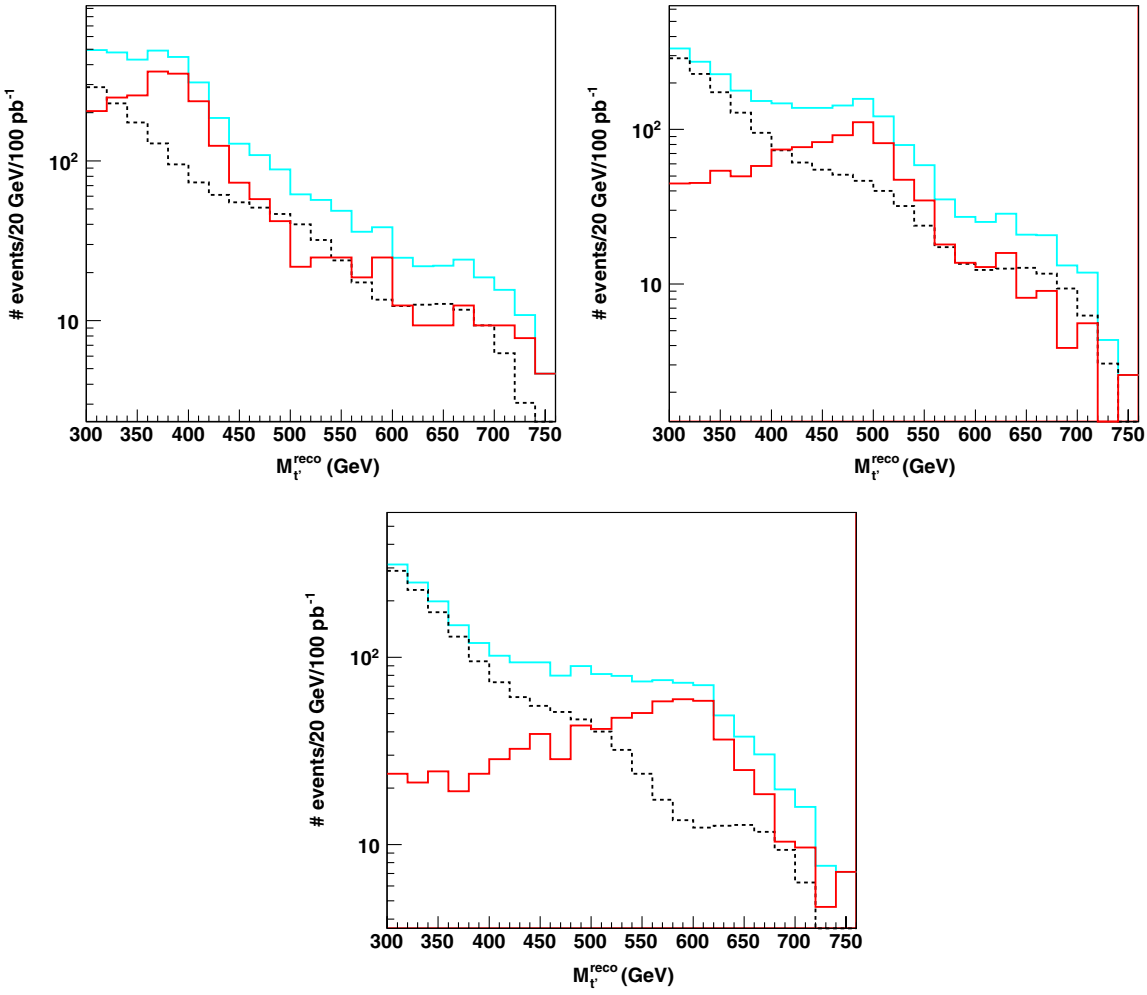

FIG. 13 (color online). Mass reconstruction of the t' signal ($b\ell\nu$) (solid line) with $\kappa/\Lambda = 0.4$ TeV^{-1} for $m_{t'} = 400$ GeV (upper-left panel), $m_{t'} = 500$ GeV (upper-right panel), and $m_{t'} = 600$ GeV (lower panel), and the corresponding background (dashed line) at $\sqrt{s} = 10$ TeV.

TABLE VII. The SS for different masses of the t' quark, where we take some anomalous parameters in the range $\kappa = 0.1$–1.0 at $\sqrt{s} = 10$ TeV and $L_{\text{int}} = 100$ pb^{-1}.

SS	$m_{t'} = 400$ GeV	$m_{t'} = 500$ GeV	$m_{t'} = 600$ GeV
$\kappa/\Lambda = 0.1$ TeV^{-1}	1.91	1.99	2.25
$\kappa/\Lambda = 0.2$ TeV^{-1}	6.95	7.19	8.11
$\kappa/\Lambda = 0.4$ TeV^{-1}	21.09	21.40	23.44
$\kappa/\Lambda = 0.6$ TeV^{-1}	41.97	38.51	38.28
$\kappa/\Lambda = 0.8$ TeV^{-1}	55.05	53.05	50.10
$\kappa/\Lambda = 1$ TeV^{-1}	65.22	63.14	59.00

and E_{had} smearing, energy deposited in towers (granularity), and tag efficiencies of the remaining detector effects such as misidentifications. More realistic simulations require the resources of the LHC collaborations and are beyond the scope of this work. The EXROOTANALYSIS package [32] is used for PGS4 data and the output is analyzed and histogrammed with the ROOT [33] macros. Since the cross section for $t' \to W^+ b$ is about 5 times larger than the $\bar{t}' \to W^- \bar{b}$ cross section, the analysis for the former process has been considered for the remainder of this study.

Typical kinematical distributions are shown in Figs. 10 and 11. In the event analysis, the signal ($t' \to W^+ b$, with $\kappa/\Lambda = 0.1$ TeV^{-1} and $m_{t'} = 400$, 500, 600 GeV) and background ($W^+ b$) are taken into account assuming the PIII parametrization. The W-boson invariant mass can be reconstructed from its leptonic or hadronic decays. For the leptonic reconstruction case, the criteria applied to the electrons or muons are $p_T^\ell > 20$ GeV and $|\eta^\ell| < 2.5$, whereas for missing transverse energy, the requirement is $\not{E}_T > 20$ GeV. For the hadronic reconstruction case, we require at least two jets with $p_T^j > 20$ GeV and $|\eta^j| < 2.5$. For the reconstruction of the t'-quark invariant mass, the b-tagged jets are required to have $p_T^{j_b} > 50$ GeV and $|\eta^{j_b}| < 2$ for both cases.

The final results are presented only for the case where the W boson is reconstructed from its leptonic decays. The four-momentum vector of the neutrino is calculated from lepton and missing transverse energy assuming a W-boson rest mass constraint. The plots for the reconstructed t' invariant mass after detector simulation are given in Fig. 12 at $\sqrt{s} = 14$ TeV and in Fig. 13 at $\sqrt{s} = 10$ TeV. We include the possible backgrounds contributing to the same final state, and count the signal (S) and background (B) events in the corresponding mass intervals to calculate the statistical significance (SS) defined as [34]

$$\text{SS} = \sqrt{2\left[(S+B)\ln\left(1+\frac{S}{B}\right) - S\right]}. \qquad (14)$$

In Table VII, the significance calculations are presented for different mass and anomalous coupling values at $\sqrt{s} = 10$ TeV. Here, we use the mass bin width $\Delta m = \max(2\Gamma, \delta m)$ to count signal and background events with the mass resolution δm. The significance increases with κ/Λ, assuming a maximal mixing between the fourth- and the third-family quarks. The results of this study show that, with early LHC data, one can discover extra up-type quarks if there is a large anomalous coupling with other up-type quarks.

VI. CONCLUSION

Anomalous interactions could become significant at tree-level processes due to possible large masses of the fourth-family quarks. The fourth-family t' quarks can be produced with large numbers if they have anomalous couplings that dominate over the SM chiral interactions. Following the results from the signal significance for t' anomalous production, the sensitivity to the anomalous coupling κ/Λ can be reached down to 0.1 TeV^{-1} in the b-jet + lepton + $\not{E}_T$ channel at $\sqrt{s} = 10$ TeV, assuming a maximal parametrization for the extended CKM elements. The LHC experiments can observe the fourth-family quarks mostly in pairs, and single in the s-channel if they have large anomalous couplings to the known quarks. If detected at the LHC experiments, the fourth-family quarks will change our perspective on the flavor and the mass.

ACKNOWLEDGMENTS

We acknowledge support from the Physics Department at CERN. The work of O. C. and H. D. Y. is supported by Turkish Atomic Energy Authority (TAEA) and Turkish State Planning Organization under Grant No. DPT2006K-120470. H. D. Y's work is also supported by TÜBİTAK Project No. 105T442. G. U.'s work is supported in part by U.S. Department of Energy Grant No. DE FG0291ER40679.

[1] C. Amsler *et al.* (Particle Data Group), Phys. Lett. B **667**, 1 (2008).
[2] P. Q. Hung and M. Sher, Phys. Rev. D **77**, 037302 (2008).
[3] Z. Murdock, S. Nandi, and Z. Tavartkiladze, Phys. Lett. B **668**, 303 (2008).
[4] G. D. Kribs, T. Plehn, M. Spannowsky, and T. M. P. Tait, Phys. Rev. D **76**, 075016 (2007); R. Fok and G. D. Kribs, Phys. Rev. D **78**, 075023 (2008).
[5] B. Holdom, J. High Energy Phys. 08 (2006) 076; 03 (2007) 063.
[6] V. A. Novikov, L. B. Okun, A. N. Rozanov, and M. I. Vysotsky, JETP Lett. **76**, 127 (2002).
[7] H.-J. He, N. Polonsky, and S. Su, Phys. Rev. D **64**, 053004 (2001).
[8] V. E. Ozcan, S. Sultansoy, and G. Unel, J. Phys. G **36**, 095002 (2009).
[9] H. Fritzsch, Phys. Lett. B **184**, 391 (1987); A. Datta, Pramana **40**, L503 (1993); A. Çelikel, A. K. Çiftçi, and S. Sultansoy, Phys. Lett. B **342**, 257 (1995).
[10] G. Bregar, M. Breskvar, D. Lukman, and N. S. Mankoc Borstnik, arXiv:0708.2846.
[11] T. Ibrahim and P. Nath, Phys. Rev. D **78**, 075013 (2008).
[12] B. Holdom, W. S. Hou, T. Hurth, M. L. Mangano, S. Sultansoy, and G. Unel, arXiv:0904.4698.
[13] CDF Collaboration, Report No. CDF/PHYS/EXO/PUBLIC/9759 (2009); CDF Collaboration, CDF Note 8495 (2007).
[14] CDF Public Note, http://www-cdf.fnal.gov/physics/new/top/2008/tprop/Tprime2.8/public.html.
[15] N. Cabibbo, Phys. Rev. Lett. **10**, 531 (1963); M. Kobayashi and T. Maskawa, Prog. Theor. Phys. **49**, 652 (1973).
[16] V. M. Abazov *et al.* (D0 Collaboration), Phys. Rev. Lett. **98**, 181802 (2007); Phys. Rev. D **78**, 012005 (2008).
[17] J. A. Herrera, R. H. Benavides, and W. A. Ponce, Phys. Rev. D **78**, 073008 (2008).
[18] M. Bobrowski, A. Lenz, J. Riedl, and J. Rohrwild, Phys. Rev. D **79**, 113006 (2009).
[19] E. Arik *et al.*, Eur. Phys. J. C **26**, 9 (2002); Phys. Rev. D **66**, 033003 (2002); E. Arik, O. Cakir, and S. Sultansoy, Phys. Rev. D **67**, 035002 (2003).
[20] A. K. Ciftci *et al.*, AIP Conf. Proc. **899**, 227 (2007); R. Ciftci, Phys. Rev. D **78**, 075018 (2008).
[21] O. Cakir *et al.*, Eur. Phys. J. C **56**, 537 (2008); arXiv:0801.0236v2.
[22] T. Aaaltonen *et al.*, Phys. Rev. Lett. **103**, 092002 (2009).
[23] M. S. Chanowitz, Phys. Rev. D **79**, 113008 (2009).
[24] V. E. Ozcan, S. Sultansoy, and G. Unel, Eur. Phys. J. C **57**, 621 (2008).
[25] H. Fritzsch and D. Holtmannspotter, Phys. Lett. B **457**, 186 (1999).
[26] E. Boos *et al.* (CompHEP Collaboration), Nucl. Instrum. Methods Phys. Res., Sect. A **534**, 250 (2004).
[27] J. Pumplin *et al.*, J. High Energy Phys. 07 (2002) 012.
[28] T. Sjostrand *et al.*, J. High Energy Phys. 05 (2006) 026.
[29] A. S. Belyaev *et al.*, arXiv:hep-ph/0101232.
[30] J. Conley, Pretty Good Simulation (PGS), http://www.physics.ucdavis.edu/~conway/research/software/pgs/pgs4-general.htm.
[31] ATLAS Collaboration, Report No. CERN/LHCC/94-43 and No. CERN/LHCC/99-14/15, 1999; CMS Collaboration, CMS TDR 8.1, Report No. CERN/LHCC 2006-001.
[32] EXROOTANALYSIS package for PGS data analysis, http://madgraph.hep.uiuc.edu/Downloads/ExRootAnalysis/.
[33] R. Brun and F. Rademakers, ROOT, An object-oriented data analysis framework, v5.22 (2009).
[34] The CMS Collaboration 2007, J. Phys. G **34**, 995 (2007).